MIM: A deep mixed residual method for solving high-order partial differential equations

Liyao Lyu[a,b], Zhen Zhang[c], Minxin Chen[a,d,*], Jingrun Chen[a,d,*]

[a]*School of Mathematical Sciences, Soochow University, Suzhou, 215006, China*
[b]*CW Chu College, Soochow University, Suzhou, 215006, China*
[c]*Nanjing TBS Information Technology Co. Ltd, Nanjing, 210000, China*
[d]*Mathematical Center for Interdisciplinary Research, Soochow University, Suzhou, 215006, China*

Abstract

In recent years, a significant amount of attention has been paid to solve partial differential equations (PDEs) by deep learning. For example, deep Galerkin method (DGM) uses the PDE residual in the least-squares sense as the loss function and a deep neural network (DNN) to approximate the PDE solution. In this work, we propose a deep mixed residual method (MIM) to solve PDEs with high-order derivatives. Notable examples include Poisson equation, Monge-Ampére equation, biharmonic equation, and Korteweg-de Vries equation. In MIM, we first rewrite a high-order PDE into a first-order system, very much in the same spirit as local discontinuous Galerkin method and mixed finite element method in classical numerical methods for PDEs. We then use the residual of first-order system in the least-squares sense as the loss function, which is in close connection with least-squares finite element method. For aforementioned classical numerical methods, the choice of trail and test functions is important for stability and accuracy issues in many cases. MIM shares this property when DNNs are employed to approximate unknowns functions in the first-order system. In one case, we use nearly the same DNN to approximate all unknown functions and in the other case, we use totally different DNNs for different unknown functions. Numerous results of MIM with different loss functions and different choice

---

*Corresponding authors.
    Email addresses: `lyuliyao@msu.edu` (Liyao Lyu), `zhangzhen@tbs-info.com` (Zhen Zhang), `chenminxin@suda.edu.cn` (Minxin Chen), `jingrunchen@suda.edu.cn` (Jingrun Chen)

of DNNs are given for four types of PDEs. In most cases, MIM provides better approximations (not only for high-derivatives of the PDE solution but also for the PDE solution itself) than DGM with nearly the same DNN and the same execution time, sometimes by more than one order of magnitude. When different DNNs are used, in many cases, MIM provides even better approximations than MIM with only one DNN, sometimes by more than one order of magnitude. Numerical observations also imply a successive improvement of approximation accuracy when the problem dimension increases and interesting connections between MIM and classical numerical methods. Therefore, we expect MIM to open up a possibly systematic way to understand and improve deep learning for solving PDEs from the perspective of classical numerical analysis.

1. Introduction

Solving partial differential equations (PDEs) has been the most ubiquitous tool to simulate complicated phenomena in applied sciences and engineering problems. Classical numerical methods include finite difference method [27], finite element method (FEM) [15], discontinuous Galerkin method [10], and spectral method [34], which are typically designed for low dimensional PDEs and are well understood in terms of stability and accuracy. However, there are high dimensional PDEs such as Schrödinger equation in the quantum many-body problem [11], Hamilton-Jacobi-Bellman equation in stochastic optimal control [1], and nonlinear Black-Scholes equation for pricing financial derivatives [23]. Solving these equations is far out of the capability of classical numerical methods due to the curse of dimensionality, i.e., the number of unknowns grows exponentially fast as the dimension increases.

Until very recently, deep-learning based methods have been developed to solving these high-dimensional PDEs; see [13, 17, 14, 18, 32, 35, 24, 33, 2, 7, 16, 25, 3, 36, 38, 12] for examples. Typically, there are three main ingredients (stages) of a deep-learning method for solving PDEs: (1) modeling: the loss (objective) function to be optimized; (2) architecture: the deep neural network (DNN) for function approximation; (3) optimization: the optimal set of parameters in the DNN which minimizes the loss function. By design, the number of parameters in DNNs grows at most polynomially in terms of dimension. Meanwhile, possibly high-dimensional integrals in the loss function are approximated by Monte-Carlo method. Therefore, by design, deep

2

learning overcomes the curse of dimensionality. In practice, deep learning performs well for Schrödinger equation [17, 19], Hamilton-Jacobi-Bellman equation [18, 13], and nonlinear Black-Scholes equation [2, 7].

Typically, deep learning solves a PDE in the following way. For the given PDE, the loss function is modeled as the equation residual in the least-squares sense [35] or the variational form if exists [14]. ResNet is often used as the network architecture [21], which was tested to overcome the notorious problem of vanishing/exploding gradient. Afterwards, stochastic gradient descent method is used to find the optimal set of parameters in ResNet which minimizes the loss function. ResNet with the optimal set of parameters gives an approximation of the PDE solution.

In this work, we propose a deep mixed residual method (MIM) for solving high-order PDEs. In the modeling stage, by rewriting a given PDE into a first-order system, we obtain a larger problem in the sense that both the PDE solution and its high-order derivatives are unknown functions to be approximated. This has analogs in classical numerical methods, such as local discontinuous Galerkin method [10] and mixed finite element method [6]. Compared to DGM, there are two more degrees of freedom in MIM:

- In the loss function stage, one can choose different high-order derivatives into the set of unknown functions. Take biharmonic equation as an example. The set of unknown functions can include the PDE solution and its derivatives up to the third order, or only contain the PDE solution and its second-order derivatives, and both choices have analogs in discontinuous Galerkin method [37, 9]. We then write the loss function as the sum of equation residuals in the least-squares sense, very much in the same spirit as the least-squares finite element method [5].

- In the architecture stage, one can choose the number of networks to approximate the set of unknown functions. In one case, one DNN is used to approximate the PDE solution and other DNNs are used to approximate its high-order derivatives; in the other case, the PDE solution and its derivatives share nearly the same DNN.

These two degrees of freedom allow MIM to produce better approximations over DGM in all examples, including Poisson equation, Monge-Ampére equation, biharmonic equation, and Korteweg-de Vries (KdV) equation. In particular, MIM provides better approximations not only for the high-order

3

derivatives but also for the PDE solution itself. It is worth mentioning that the usage of mixed residual in deep learning was first introduced for surrogate modeling and uncertainty quantification of a second-order elliptic equation [39] and was later adopted in a deep domain decomposition method [28].

The paper is organized as follows. In Section 2, we introduce MIM and DGM (for comparison purpose). In Section 3, numerical results for four types of high-order PDEs are provided. Conclusions and discussions are drawn in Section 4.

2. Deep mixed residual method

In this section, we introduce MIM and discuss its difference with DGM in terms of loss function and neural network structure.

2.1. Loss function

Consider a potentially time-dependent nonlinear PDE over a bounded domain $\Omega \subset \mathbb{R}^d$

$$\begin{cases} \partial_t u + \mathcal{L}u = 0 & (t, x) \in (0, T] \times \Omega, \\ u(0, x) = u_0(x) & x \in \Omega, \\ u(t, x) = g(x) & (t, x) \in [0, T] \times \partial\Omega, \end{cases} \tag{1}$$

where $\partial\Omega$ denotes the boundary of Ω. In DGM, the loss function is defined as the PDE residual in the least-squares sense

$$L(u) = \|\partial_t u + \mathcal{L}u\|_{2,[0,T]\times\Omega}^2 + \lambda_1 \|u(0, x) - u_0\|_{2,\Omega}^2 + \lambda_2 \|u - g\|_{2,[0,T]\times\partial\Omega}^2, \tag{2}$$

where λ_1 and λ_2 are penalty parameters given *a priori*. These three terms in (2) measure how well the approximate solution satisfies the PDE, the initial condition and the boundary condition, respectively.

In the absence of temporal derivatives, (1) reduces to

$$\begin{cases} \mathcal{L}u = 0 & x \in \Omega, \\ u(x) = g(x) & x \in \partial\Omega, \end{cases}$$

and the corresponding loss function in DGM becomes

$$L(u) = \|\mathcal{L}u\|_{2,\Omega}^2 + \lambda \|u - g\|_{2,\partial\Omega}^2. \tag{3}$$

Equation	Explicit form	Loss function $L(u)$
Poisson	$-\Delta u = f(x)$	$\|\Delta u + f(x)\|_{2,\Omega}^2$
Monge-Ampére	$\det(\nabla^2 u) = f(x)$	$\|\det(\nabla^2 u) - f(x)\|_{2,\Omega}^2$
Biharmonic	$-\Delta^2 u = f(u,x)$	$\|\Delta^2 u + f(u,x)\|_{2,\Omega}^2$
KdV	$u_t + \sum_{i=1}^d u_{x_i x_i x_i} = f(x)$	$\|u_t + \sum_{i=1}^d u_{x_i x_i x_i} - f(x)\|_{2,\Omega}^2$

Table 1: Loss functions for four types of PDEs in the deep Galerkin method.

Condition	Explicit form	Contribution to the loss function
Dirichlet	$u(x) = g$	$\|u - g\|_{2,[0,T]\times\partial\Omega}^2$
Neumann	$\frac{\partial u}{\partial n} = g$	$\|\frac{\partial u}{\partial n} - g\|_{2,[0,T]\times\partial\Omega}^2$ or $\|p - g\|_{2,[0,T]\times\partial\Omega}^2$
Initial	$u(0,x) = u_0(x)$	$\|u - u_0\|_{2,\Omega}^2$

Table 2: Contributions to the loss function for the initial condition and different types of boundary conditions used in the deep Galerkin method and the deep mixed residual method.

Table 1 lists four PDEs with their corresponding loss functions in DGM and Table 2 lists different boundary conditions, the initial condition and their contributions to loss functions in DGM and MIM. More boundary conditions can be treated in this way. Interested readers may refer to [8] for details.

In MIM, we first rewrite high-order derivatives into low-order ones using auxiliary variables. For notational convenience, auxiliary variables p, q, w represent

$$
\begin{aligned}
p &= \nabla u, \\
q &= \nabla \cdot p = \Delta u, \\
w &= \nabla q = \nabla(\Delta u).
\end{aligned}
\tag{4}
$$

For KdV equation, we have $q = \mathrm{diag}(\nabla p)$ instead of the second formula in (4). With these auxiliary variables, we define loss functions for four types of PDEs in Table 3. Since one can choose a subset of high-order derivatives into the set of unknown functions, there are more than one loss function in MIM. For biharmonic equation, there are two commonly used sets of auxiliary variables in local discontinuous Galerkin method and weak Galerkin finite element method: one with all high-order derivatives [37] and the other with part of high-order derivatives [9, 30]. Correspondingly, if all high-order derivatives are used, we denote MIM by MIM_a, and if only part of high-order derivatives are used, we denote MIM by MIM_p. In Section 2.2, we will discuss how to equip different loss functions with different DNNs. In short, if only one DNN

5

is used to approximate the PDE solution and its derivatives, we denote MIM by MIM^1, and if multiple DNNs are used, we denote MIM by MIM^2. In Section 3, different loss functions listed in Table 1, Table 2 and Table 3 will be tested and discussed. By default, all the penalty parameters are set to be 1.

Equation	Explicit form	Loss function $L(u, p, q, w)$
Poisson	$-\Delta u = f(u, x)$	$\|p - \nabla u\|_{2,\Omega}^2 + \|\nabla \cdot p + f(u, x)\|_{2,\Omega}^2$
Monge-Ampére	$\det(\nabla^2 u) = f$	$\|p - \nabla u\|_{2,\Omega}^2 + \|\det(\nabla p) - f\|_{2,\Omega}^2$
Biharmonic	$-\Delta^2 u = f(u, x)$	$\|p - \nabla u\|_{2,\Omega}^2 + \|q - \nabla \cdot p\|_{2,\Omega}^2$ $+\|w - \nabla q\|_{2,\Omega}^2 + \|\nabla \cdot w + f\|_{2,\Omega}^2$
		$\|q - \Delta u\|_{2,\Omega}^2 + \|\Delta q + f\|_{2,\Omega}^2$
KdV	$u_t + \sum_{i=1}^d u_{x_i x_i x_i} = f(x)$	$\|p - \nabla u\|_{2,[0,T]\times\Omega}^2 + \|q - \text{diag}(\nabla p)\|_{2,[0,T]\times\Omega}^2$ $+\|u_t + \nabla \cdot q - f(x)\|_{2,[0,T]\times\Omega}^2$

Table 3: Loss functions in the deep mixed residual method for four types of equations. Two different loss functions for biharmonic equation are denoted by MIM_a and MIM_p, in which all high-order derivatives or part of high-order derivatives are included, respectively.

2.2. Neural network architecture

ResNet [21] is used to approximate the PDE solution and its high-order derivatives. It consists of m blocks in the following form

$$s_k = \sigma(W_{2,k}\sigma(W_{1,k}s_{k-1} + b_{1,k}) + b_{2,k}) + s_{k-1}, \quad k = 1, 2, \cdots, m. \quad (5)$$

Here $s_k, b_{1,k}, b_{2,k} \in \mathbb{R}^n$, $W_{1,k}, W_{2,k} \in \mathbb{R}^{n \times n}$. m is the depth of network, n is the width of network, and σ is the (scalar) activation function. Explicit formulas of activation functions used in this work are given in Table 4. The last term on the right-hand side of (5) is called the shortcut connection or residual connection. Each block has two linear transforms, two activation functions, and one shortcut; see Figure 1 for demonstration. Such a structure can automatically solve the notorious problem of vanishing/exploding gradient [22].

Since x is in $\mathbb{R}^d$ rather than $\mathbb{R}^n$, we can pad x by a zero vector to get the network input s_0. A linear transform can be used as well without much difference. Meanwhile, s_m has n outputs which cannot be directly used for the PDE solution and its derivatives employed in the loss function. Therefore, a linear transform T is applied to s_m to transform it into a suitable dimension. Let $\{\theta\}$ be the whole set of parameters which include parameters in ResNet

6

Activation function	Formula
Square	x^2
ReLU	$\max\{x, 0\}$
ReQU	$(\max\{x, 0\})^2$
ReCU	$(\max\{x, 0\})^3$

Table 4: Activation functions used in numerical tests.
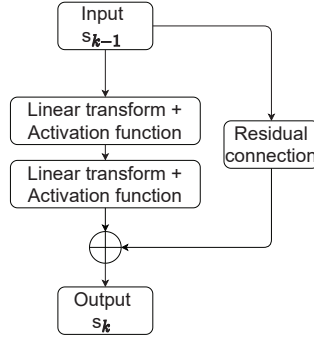
Figure 1: One block of ResNet. A deep neural network contains a sequence of blocks, each of which consists of two fully-connected layers and one shortcut connection.

$(\{W_{1,k}, b_{1,k}, W_{2,k}, b_{2,k}\}_{k=1}^{m})$ and parameters in the linear transform T. Note that the output dimension in MIM depends on both the PDE problem and the mixed residual loss. We illustrate network structures for biharmonic equation as an example in Figure 2. From Figure 2, we see that DGM has only 1 output, MIM_a^1 has $2d + 2$ outputs, and MIM_p^1 has 2 outputs. In Figure 3, we illustrate networks structures of MIM^1 and MIM^2 for Poisson equation. In MIM^2, two DNNs are used: one to approximate the solution and the other one to approximate its derivatives. It is clear from Figure 2 that network structures in DGM and MIM^1 only differ in the output layer and thus they have comparable numbers of parameters to be optimized. To be precise, we calculate their numbers of parameters in Table 5, from which one can see the number of parameters in DGM and MIM^1 is close. The number of parameters in MIM^2 is nearly double for Poisson equation, Monge-Ampére equation and biharmonic equation (MIM_p^2), tripled for KdV equation, and quadrupled for biharmonic equation (MIM_a^2), respectively. In Section 3, from numerical results, we observe a better performance of MIM^1 for all four equations, not only for derivatives of the PDE solution, but also for the solution itself.
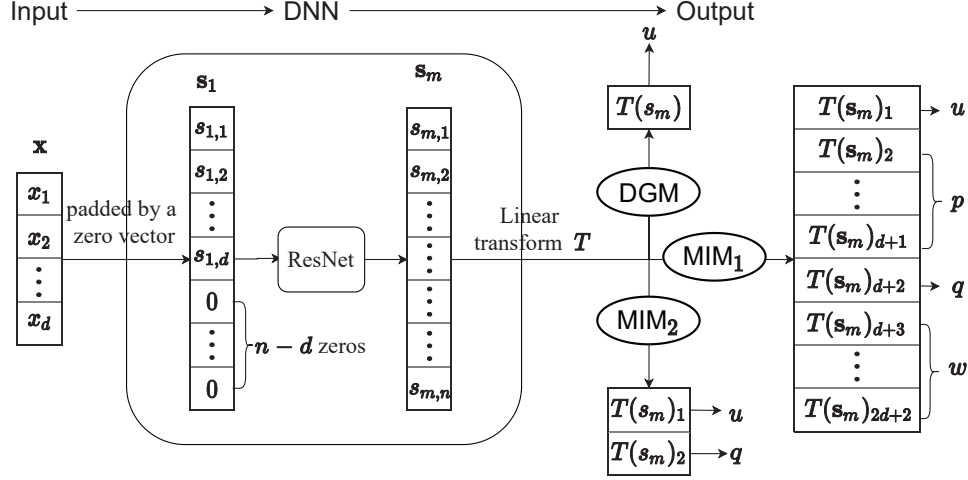
Figure 2: Network structures for biharmonic equation with deep Galerkin method and deep mixed residual method. DGM only approximates solution u. MIM_p^1 approximate solution u and Δu. MIM_a^1 approximates solution u and all of its derivatives used in the equation $\nabla u, \Delta u, \nabla(\Delta u)$. MIM_a^2 uses four networks to approximate $u, \nabla u, \Delta u, \nabla(\Delta u)$ and MIM_p^2 uses two networks to approximate $u, \Delta u$. Each network has a similar structure with different output dimensions.

Method	Equation	Size of the parameter set
DGM	Four equations	$(2m-1)n^2 + (2m+d+1)n + 1$
MIM^1	Poisson	$(2m-1)n^2 + (2m+2d+1)n + d + 1$
	Monge-Ampére	
	Biharmonic (MIM$_a^1$)	$(2m-1)n^2 + (2m+3d+2)n + 2d + 2$
	Biharmonic (MIM$_p^1$)	$(2m-1)n^2 + (2m+d+2)n + 2$
	KdV	$(2m-1)n^2 + (2m+3d+1)n + 2d + 1$
MIM^2	Poisson	$(4m-2)n^2 + (4m+3d+1)n + d + 1$
	Monge-Ampére	
	Biharmonic (MIM$_a^2$)	$(8m-4)n^2 + (8m+6d+2)n + 2d + 2$
	Biharmonic (MIM$_p^2$)	$(4m-2)n^2 + (4m+2d+2)n + 2$
	KdV	$(6m-3)n^2 + (6m+5d+1)n + 2d + 1$

Table 5: Number of parameters for different network structures used for different equations and different loss functions. n, m, and d are the network width, the network depth, and the problem dimension, respectively. It is observed that the number of parameters in DGM and MIM^1 is close, and the number of parameters in MIM^2 is nearly double for Poisson equation, Monge-Ampére equation and biharmonic equation (MIM$_p^2$), tripled for KdV equation, and quadrupled for biharmonic equation (MIM$_a^2$), respectively.

8

Quantity	DGM	MIM
u	$\dfrac{\int_\Omega (u_\theta - u)^2 dx}{\int_\Omega u^2 dx}$	$\dfrac{\int_\Omega (u_\theta - u)^2 dx}{\int_\Omega u^2 dx}$
∇u	$\dfrac{\int_\Omega (\nabla u_\theta - \nabla u)^2 dx}{\int_\Omega (\nabla u)^2 dx}$	$\dfrac{\int_\Omega (p_\theta - \nabla u)^2 dx}{\int_\Omega (\nabla u)^2 dx}$
Δu	$\dfrac{\int_\Omega (\Delta u_\theta - \Delta u)^2 dx}{\int_\Omega (\Delta u)^2 dx}$	$\dfrac{\int_\Omega (q_\theta - \Delta u)^2 dx}{\int_\Omega (\Delta u)^2 dx}$
$\nabla \Delta u$	$\dfrac{\int_\Omega (\nabla(\Delta u_\theta) - \nabla(\Delta u))^2 dx}{\int_\Omega (\nabla(\Delta u))^2 dx}$	$\dfrac{\int_\Omega (w_\theta - \nabla(\Delta u))^2 dx}{\int_\Omega (\nabla(\Delta u))^2 dx}$
$\mathrm{diag}(\nabla^2 u)$	$\dfrac{\int_\Omega (\mathrm{diag}(\nabla^2 u_\theta) - \mathrm{diag}(\nabla^2 u))^2 dx}{\int_\Omega (\mathrm{diag}(\nabla^2 u))^2 dx}$	$\dfrac{\int_\Omega (q_\theta - \mathrm{diag}(\nabla^2 u))^2 dx}{\int_\Omega (\mathrm{diag}(\nabla^2 u))^2 dx}$

Table 6: Relative L^2 errors used in deep Galerkin method and deep mixed residual method.

2.3. Stochastic Gradient Descent

For completeness, we also briefly introduce stochastic gradient descent method. For the loss function defined in (3), we generate two sets of points uniformly distributed over Ω and $\partial\Omega$: $\{\mathbf{x}_i\}_{i=1}^N$ in Ω and $\{\hat{\mathbf{x}}_j\}_{j=1}^M$ on $\partial\Omega$.

$$\theta^{k+1} = \theta^k - \alpha \nabla_\theta \frac{|\Omega|}{N} \sum_{i=1}^N [\mathcal{L}u_\theta(\mathbf{x}_i; \theta^k)]^2 + \lambda\alpha\nabla_\theta \frac{|\partial\Omega|}{M} \sum_{j=1}^M [u_\theta(\hat{\mathbf{x}}_j; \theta^k) - g(\hat{\mathbf{x}}_j)]^2,$$

(6)

where α is the learning rate chosen to be $1e-3$ here. $|\Omega|$ and $|\partial\Omega|$ are measures of Ω and $\partial\Omega$, respectively. u_θ is the DNN approximation of PDE solution parameterized by $\{\theta\}$. Sampling points $\{\mathbf{x}_i\}_{i=1}^N$ and $\{\hat{\mathbf{x}}_j\}_{j=1}^M$ are updated at each iteration. In implementation, we use ADAM optimizer [26] and automatic differentiation [31] for derivatives in PyTorch.

3. Numerical Result

In this section, we show numerical results of MIM for four types of equations. We use relative L^2 errors of u, ∇u, Δu, and $\nabla(\Delta u)$ defined in Table 6 for comparison. In all figures, relative L^2 errors are in $\log_{10}$ scale.

3.1. Poisson Equation

Consider the following Neumann problem

$$\begin{cases} -\Delta u + \pi^2 u = 2\pi^2 \sum_{k=1}^d \cos(\pi x_k) & x \in \Omega = [0,1]^d \\ \dfrac{\partial u}{\partial n} = 0 & x \in \partial\Omega \end{cases}$$

(7)

9

with the exact solution $u(x) = \sum_{k=1}^{d} \cos(\pi x_k)$. The neural network structure in DGM is the same as that for biharmonic equation shown in Figure 2. Following Table 1 and Table 2, we use the loss function for (7)

$$L(u) = \| - \Delta u + \pi^2 u - 2\pi^2 \sum_{k=1}^{d} \cos(\pi x_k) \|_{2,\Omega}^2 + \lambda \| \frac{\partial u}{\partial n} \|_{2,\partial\Omega}^2. \tag{8}$$

Since both u and p are explicitly used, one more advantage of MIM is the enforcement of boundary conditions. For (7), we multiply p_i, $i = 1, \cdots, d$ by $x_i(1 - x_i)$ to satisfy the Neumann boundary condition automatically; see Figure 3. DGM only has u as its unknown function, and thus it is unclear that how the exact Neumann boundary condition can be imposed. Therefore, for DNNs in Figure 3, the loss function in MIM can be simplified as

$$L(u, p) = \| p - \nabla u \|_{2,\Omega}^2 + \| - \nabla \cdot p + \pi^2 u - 2\pi^2 \sum_{k=1}^{d} \cos(\pi x_k) \|_{2,\Omega}^2. \tag{9}$$

We emphasize that Dirichlet boundary condition can be exactly imposed in DGM [4] and no penalty term is needed. For Neumann boundary condition, mixed boundary condition, and Robin boundary condition, however, it is difficult to build up a DNN representation which satisfies the exact boundary condition. Building up a DNN approximation which satisfies the exact boundary condition can have a couple of advantages [8]: 1) make ease of the training process by avoiding unnecessary divergence; 2) improve the approximation accuracy; 3) save the execution time. In MIM, however, we have the direct access to both u and p. Therefore, all these boundary conditions can be imposed exactly in principle. This will be presented in a subsequent work [29].

For (7), average errors of u and ∇u over the last 100 iterations are recorded in Table 7. The network depth $m = 2$ and the activation function x^2 is used. Network widths are $5, 10, 15, 20$ for $2, 4, 8, 16$ dimensional problems, respectively. Time is recorded as the average CPU time per iteration. It is not surprising that MIM^1 costs less time than DGM since the DNN approximation in MIM satisfies the Neumann boundary condition automatically and both methods have similar network structures. It is surprising that MIM^2 costs less time than DGM since the number of parameters in MIM^2 is about twice of that in DGM. In terms of execution time, $\text{MIM}^1 < \text{MIM}^2 <$ DGM. Figure 4 and Figure 5 plot training processes of DGM and MIM in
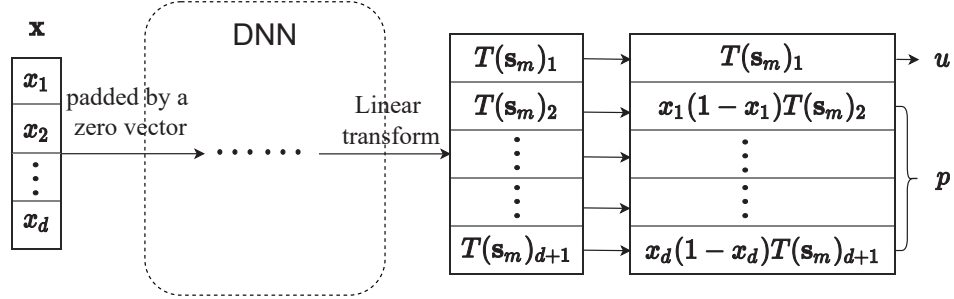
(a) MIM^1: one network to approximate the PDE solution and its derivatives.
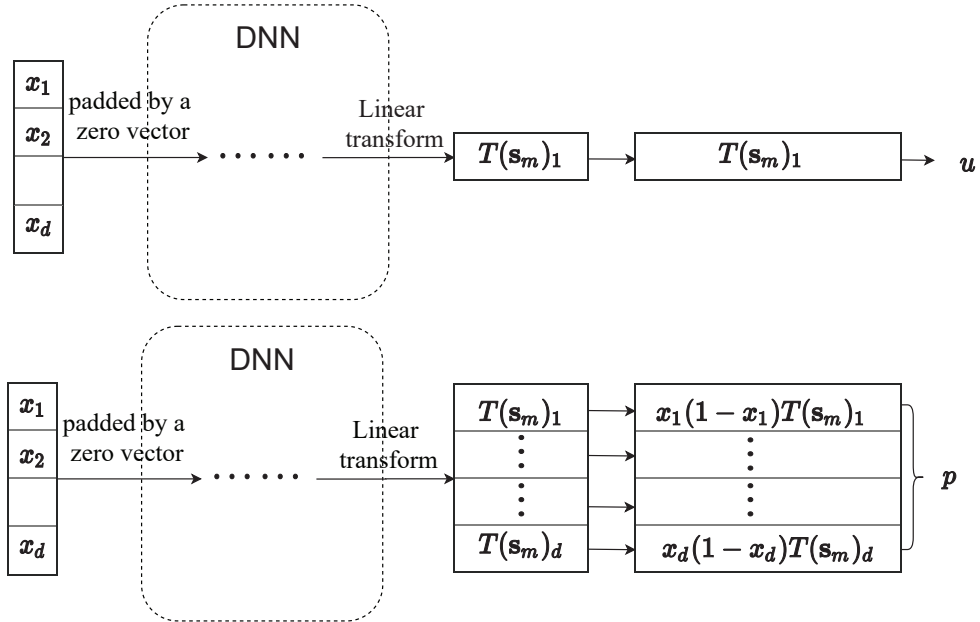
(b) MIM^2: multiple networks to appriximate the PDE solution and its derivatives.

Figure 3: Detailed network structures of MIM^1 and MIM^2 to solve Poisson equation. DNN part is the same as that in Figure 2. $x_i(1 - x_i)$ are multipliers which make MIM^1 and MIM^2 satisfy the exact Neumann boundary condition.

d	Method	Relative L^2 error ($\times 10^{-2}$)		Time (s)
		u	∇u	
	DGM	0.3676	0.3714	0.04374
2	MIM^1	0.2941	0.1639	0.02925
	MIM^2	0.0565	0.0236	0.03514
	DGM	1.0022	1.3272	0.07455
4	MIM^1	0.3751	0.3290	0.03603
	MIM^2	0.2294	0.0690	0.04141
	DGM	2.0022	2.6551	0.13081
8	MIM^1	0.9049	0.6423	0.06642
	MIM^2	0.7261	0.1499	0.08716
	DGM	3.9796	5.0803	0.25621
16	MIM^1	1.7631	1.0041	0.11082
	MIM^2	0.0787	0.0236	0.15125

Table 7: Relative errors for u and ∇u in DGM and MIM for Poisson equation defined in (7).

terms of relative L^2 errors for u and ∇u. Generally speaking, in terms of approximation error, MIM^2 < MIM^1 < DGM as expected. Therefore, MIM provides a better strategy over DGM. MIM provides better approximations in terms of relative L^2 errors for both u and ∇u. For ∇u, the improvement of MIM^1 over DGM is about several times and that of MIM^2 over MIM^1 is about one order of magnitude. For u, the improvement is about several times. Moreover, a dimensional dependence is observed for both u and ∇u. The higher the dimension is, the better the approximation is.

Table 8 records approximation errors of MIM and DGM in terms of activation function and network depth when $d = 4$. MIM provides better approximations for both ∇u and u. It is not surprising that ReLU is not a suitable function for DGM due to high-order derivatives, but is suitable in MIM since only first-order derivatives are present in MIM.

3.2. Monge-Ampére equation

Consider the nonlinear Monge-Ampére equation

$$\begin{cases} \det(\nabla^2 u) = f(x) & x \in \Omega = [-1,1]^d \\ u(x) = g(x) & x \in \partial\Omega \end{cases} \tag{10}$$

12
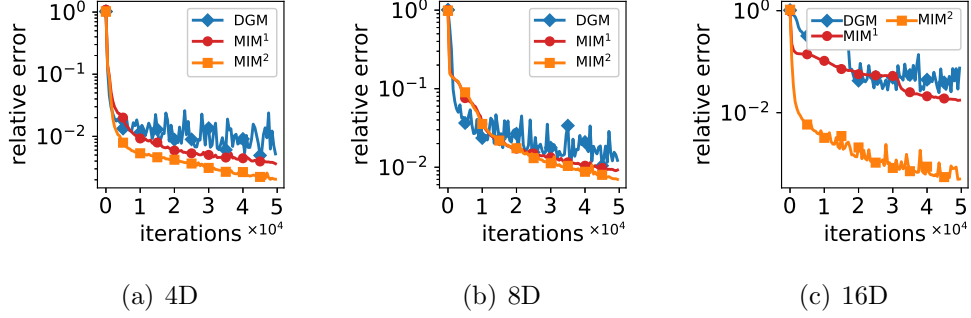
Figure 4: Relative L^2 error of u in terms of iteration number for Poisson equation defined in (7).
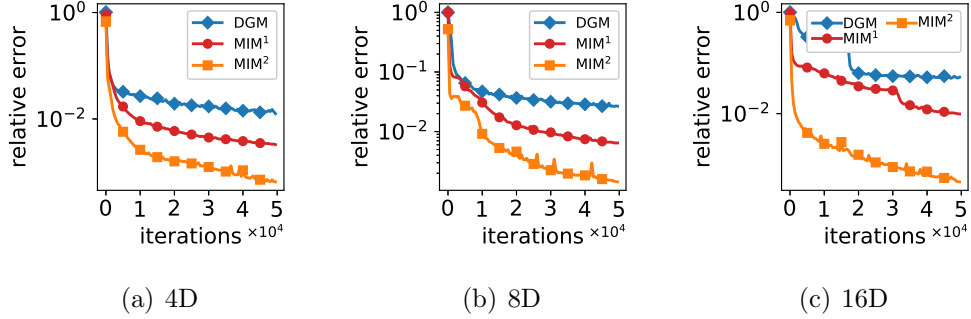
Figure 5: Relative L^2 error of ∇u in terms of iteration number for Poisson equation defined in (7).

with the exact solution defined as $u(x) = e^{1/d(\sum_{i=1}^{d} x_i^2)}$. Following Table 1, 3 and 2, we have the loss function in DGM

$$L(u) = \|\det(\nabla^2 u) - f\|_{2,\Omega}^2 + \lambda \|u - g\|_{2,\partial\Omega}^2,$$

and the loss function in MIM

$$L(u, p) = \|p - \nabla u\|_{2,\Omega}^2 + \|\det(\nabla p) - f\|_{2,\Omega}^2 + \lambda \|u - g\|_{2,\partial\Omega}^2,$$

respectively. For (10), the Dirichlet boundary condition can be enforced for both DGM and MIM. For comparison purpose, instead, we have the penalty term in both DGM and MIM. However, imposing exact boundary conditions is always encouraged in practice.

13

σ	m	Relative L^2 error ($\times 1$)					
		DGM		MIM[1]		MIM[2]	
		u	∇u	u	∇u	u	∇u
ReLU	1	0.9197	0.9259	0.0890	0.0444	0.0264	0.0080
	2	0.9210	0.9230	0.0245	0.0104	0.0265	0.0068
	3	0.9208	0.9216	0.0258	0.0113	0.0258	0.0084
ReQU	1	0.0684	0.1003	0.0182	0.0127	0.0107	0.0042
	2	0.0057	0.0118	0.0113	0.0047	0.0049	0.0017
	3	0.0124	0.0140	0.0040	0.0029	0.0042	0.0031
ReCU	1	0.4642	0.4644	0.0288	0.0159	0.0100	0.0033
	2	0.0281	0.0170	0.0071	0.0055	0.0048	0.0013
	3	0.0028	0.0031	0.0049	0.0036	0.0049	0.0013

Table 8: Performance of MIM and DGM with respect to network depth and activation function for Poisson equation when $d = 4$. Network width is fixed to be 10.

In this example, we fix the network depth $m = 2$ and the activation function as $\sigma(x) = \text{ReQU}(x)$. Relative L^2 errors in the last 1000 iterations with respect to the network width in different dimensions are recorded in Table 9. Figure 6 plots errors in terms of network width for different dimensions. The advantage of MIM is obvious from these results.

3.3. Biharmonic equation

Consider the biharmonic equation

$$
\begin{cases}
\Delta^2 u = \dfrac{\pi^4}{16} \displaystyle\sum_{k=1}^{d} \sin(\dfrac{\pi}{2}x) & x \in \Omega \\[2ex]
u(x) = \displaystyle\sum_{k=1}^{d} \sin(\dfrac{\pi x}{2}) & x \in \partial\Omega \\[2ex]
\dfrac{\partial u}{\partial n} = 0 & x \in \partial\Omega
\end{cases}
\tag{11}
$$

with the exact solution $u(x) = \sum_{k=1}^{d} \sin(\frac{\pi x}{2})$ over $\Omega = [-1, 1]^d$. The loss function in DGM is

$$
L(u) = \|\Delta^2 u - \frac{\pi^4}{16} \sum_{k=1}^{d} \sin(\frac{\pi}{2}x)\|_{2,\Omega}^2 + \lambda_1 \|u - \sum_{k=1}^{d} \sin(\frac{\pi x}{2})\|_{2,\partial\Omega}^2 + \lambda_2 \|\frac{\partial u}{\partial n}\|_{2,\partial\Omega}^2.
$$

d	n	DGM		MIM[1]		MIM[2]	
		u	∇u	u	∇u	u	∇u
	10	0.1236	0.7430	0.1023	0.3433	0.1251	0.5218
2	20	1.1100	3.1940	0.0922	0.3804	0.0784	0.0221
	30	0.0913	0.5656	0.0522	0.1740	0.1075	0.0219
	20	0.0981	0.7764	0.1095	0.6359	0.1230	0.3977
4	30	0.0921	0.7731	0.0903	0.4399	0.1063	0.2802
	40	0.0943	0.6174	0.0636	0.3127	0.1287	0.2480
	30	0.3584	3.3902	0.1435	1.6318	0.1155	0.5170
8	40	0.1179	1.4663	0.1344	1.0721	0.1330	0.4873
	50	0.0997	1.2483	0.0977	0.8289	0.0917	0.4174

Above header spanning: Relative L^2 error ($\times 10^{-2}$)

Table 9: Relative L^2 errors in the last 1000 iterations with respect to the network width for Monge-Ampére equation defined in (10) for different dimensions. The network depth is fixed to be $m = 2$ and the activation function is fixed to be $\sigma(x) = \mathrm{ReQU}(x)$.

The loss function in MIM_a is

$$L(u, p, q, w) = \|p - \nabla u\|_{2,\Omega}^2 + \|q - \nabla \cdot p\|_{2,\Omega}^2 + \|w - \nabla q\|_{2,\Omega}^2$$

$$+ \|\nabla \cdot w - \frac{\pi^4}{16} \sum_{k=1}^{d} \sin(\frac{\pi}{2}x)\|_{2,\Omega}^2 + \lambda_1 \|u - \sum_{k=1}^{d} \sin(\frac{\pi x}{2})\|_{2,\partial\Omega}^2 + \lambda_2 \|p\|_{2,\partial\Omega}^2, \tag{12}$$

and the loss function in MIM_p is

$$L(u, q) = \|q - \Delta u\|_{2,\Omega}^2 + \|\Delta q - \frac{\pi^4}{16} \sum_{k=1}^{d} \sin(\frac{\pi}{2}x)\|_{2,\Omega}^2$$

$$+ \lambda_1 \|u - \sum_{k=1}^{d} \sin(\frac{\pi x}{2})\|_{2,\partial\Omega}^2 + \lambda_2 \|\frac{\partial u}{\partial n}\|_{2,\partial\Omega}^2. \tag{13}$$

Again, we can enforce the exact boundary condition in MIM but cannot enforce it in DGM. For comparison purpose, we use penalty terms in both methods.

Set $m = 2$ and $n = 8, 10, 20$ when $d = 2, 4, 8$, respectively. Table 10 records averaged errors in the last 1000 iterations. Relative L^2 errors for u, ∇u, Δu and $\nabla(\Delta u)$ in terms of iteration number are plotted in Figure 7 when

(a) 2D   (b) 4D   (c) 8D

(d) 2D   (e) 4D   (f) 8D
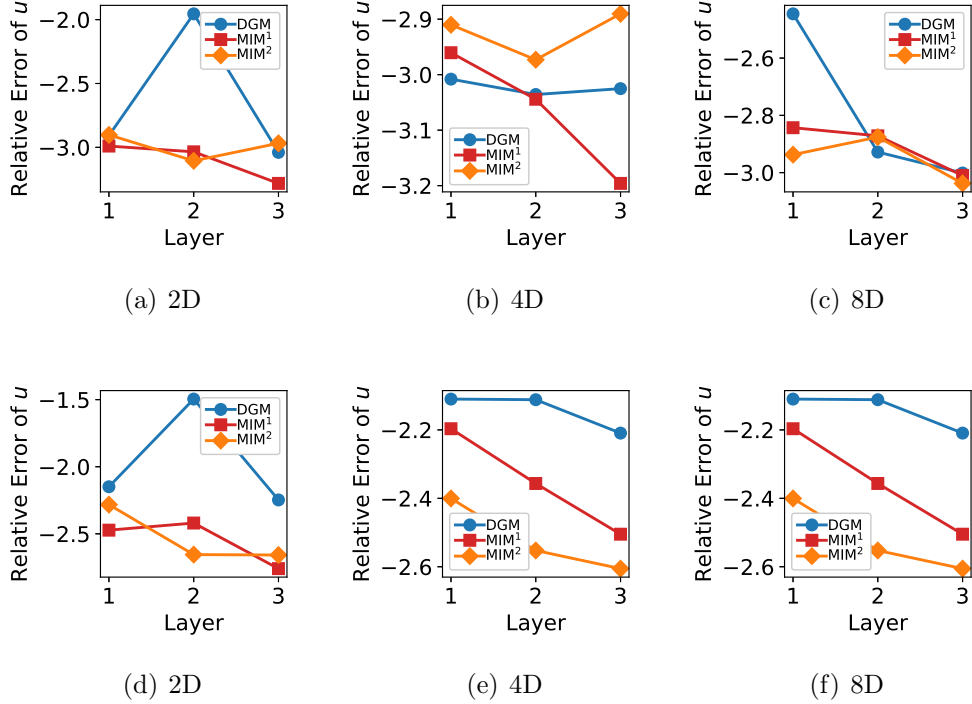
Figure 6: Relative L^2 errors of u and ∇u for Monge-Ampére equation defined in (7).

$d = 2$. Generally speaking, MIM provides better approximations for u, ∇u, Δu, and $\nabla(\Delta u)$ than DGM. For MIM_a and MIM_p, MIM_p has a slightly better approximation accuracy comparable to that of MIM_a, although MIM_a has $2d + 2$ more outputs. These results are of interests since they are connected with results of local discontinuous Galerkin method that the formulation with a subset of derivatives has a better numerical performance [37, 9]. We point out that MIM_a has the advantage that the exact boundary condition can be enforced, although we use penalty terms for this example.

(a) u

(b) ∇u
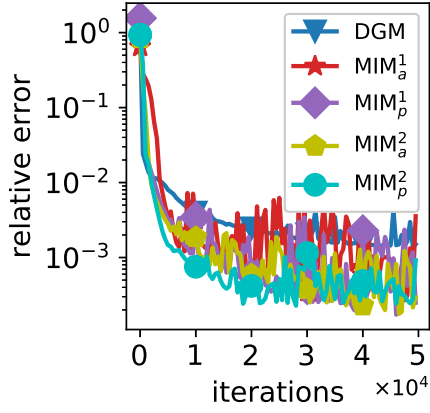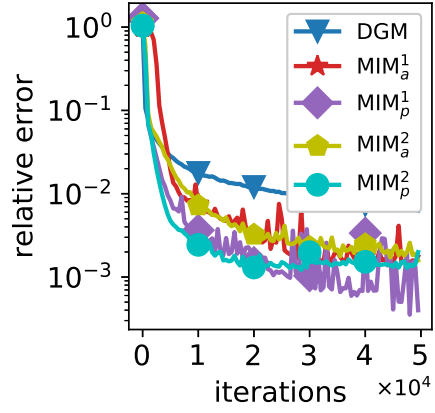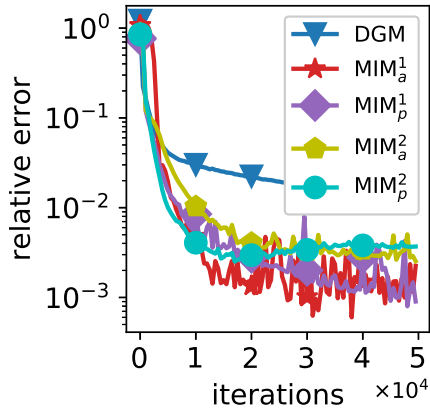
(c) Δu
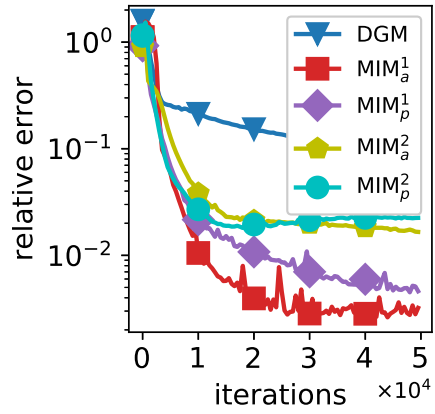
(d) $\nabla \Delta u$

Figure 7: Relative L^2 errors of u, ∇u, Δu, $\nabla(\Delta u)$ in terms of iteration number for biharmonic equation. Both the solution and its derivatives are approximated by the same network in MIM^1, while different networks are used for the solution and its derivatives in MIM^2. MIM_a means all derivatives are approximated and MIM_p means only a subsect of derivatives (Δu here) are approximated.

17

d	Method	Relative L^2 error ($\times 10^{-2}$)				Time (s)
		u	∇u	Δu	$\nabla(\Delta u)$	
	DGM	0.1656	0.6454	1.2333	8.8001	0.1034
	MIM_a^1	0.1501	0.1929	0.1564	0.3067	0.1219
2	MIM_p^1	0.0769	0.1155	0.1504	0.4984	0.1636
	MIM_a^2	0.0526	0.2066	0.2937	1.6821	0.1393
	MIM_p^2	0.0424	0.1417	0.3625	2.2231	0.2164
	DGM	0.1330	0.6454	1.2333	8.8008	0.3292
	MIM_a^1	0.4117	0.1929	0.1563	0.3066	0.2784
4	MIM_p^1	0.0845	0.1155	0.1504	0.4984	0.4692
	MIM_a^2	0.1039	0.2066	0.2937	1.6821	0.2883
	MIM_p^2	0.1111	0.1417	0.3625	2.2301	0.5919
	DGM	0.2488	1.0514	1.4594	13.4003	0.3292
	MIM_a^1	0.3719	2.3855	0.6797	3.1015	0.2784
8	MIM_p^1	0.1856	0.6909	0.7840	4.7209	0.4692
	MIM_a^2	0.1475	1.6657	1.2922	6.9594	0.8051
	MIM_p^2	0.2881	0.9223	0.9981	6.4658	6.5148

Table 10: Relative errors for biharmonic equation defined in (11). MIM_a and MIM_b represent MIM with loss functions defined in (12) and (13), respectively.

3.4. KdV equation

Consider a time-dependent linear KdV-type equation

$$
\begin{cases}
u_t + \sum_{k=1}^{d} u_{x_k x_k x_k} = 0 & (t, x) \in [0, T] \times \Omega \\
u(0, x) = u_0(x) = \sin\left(\sum_{k=1}^{d} x_k\right) & (t, x) \in [0] \times \Omega \\
u(t, x) \text{ is periodic in } x
\end{cases}
\tag{14}
$$

defined over $\Omega = [0, 2\pi]^d$, where the exact solution $u(t, x) = \sin(\sum_{k=1}^{d} x_k + dt)$. We first rewrite it into the first-order system

$$
\begin{aligned}
p &= \nabla u, \\
q &= \text{diag}(\nabla p), \\
u_t + \nabla \cdot q &= 0.
\end{aligned}
$$

18

The loss function in DGM is

$$L(u) = \|u_t + \sum_{k=1}^{d} u_{x_k x_k x_k}\|_{2,[0,1]\times\Omega}^2 + \lambda_1 \|u - \sin(\sum_{k=1}^{d} x_k + dt)\|_{2,[0,1]\times\partial\Omega}^2$$

$$+ \lambda_2 \left(\sum_{k=1}^{d} \|u(x,t) - u(x \pm 2\pi e_k, t)\|_{2,\Omega}^2 \right)$$

$$+ \lambda_3 \left(\sum_{k=1}^{d} \|\nabla u(x,t) - \nabla u(x \pm 2\pi e_k, t)\|_{2,\Omega}^2 \right).$$

Here $\{e_k\}_{k=1}^{d}$ is the standard basis set of $\mathbb{R}^d$. The loss function in MIM is

$$L(u, p, q) = \|p - \nabla u\|_{2,[0,1]\times\Omega}^2 + \|q - \text{diag}(\nabla p)\|_{2,[0,1]\times\Omega}^2$$

$$+ \|u_t + \nabla \cdot q\|_{2,[0,1]\times\Omega}^2 + \lambda_1 \|u - \sin(\sum_{k=1}^{d} x_k + dt)\|_{2,[0,1]\times\partial\Omega}^2$$

$$+ \lambda_2 \left(\sum_{k=1}^{d} \|u(x,t) - u(x \pm 2\pi e_k, t)\|_{2,\Omega}^2 \right)$$

$$+ \lambda_3 \left(\sum_{k=1}^{d} \|p(x,t) - p(x \pm 2\pi e_k, t)\|_{2,\Omega}^2 \right).$$

Relative L^2 errors of u, ∇u, and $\text{diag}(\nabla^2 u)$ are recorded in Table 11. Again, as shown in previous examples, MIM provides better results compared to DGM, especially for ReQU activation function. No obvious improvement of MIM^2 over MIM^1 is observed.

4. Conclusion and Discussion

Motivated by classical numerical methods such as local discontinuous Galerkin method, mixed finite element method, and least-squares finite element method, we develop a deep mixed residual method to solve high-order PDEs in this paper. The deep mixed residual method inherits several advantages of classical numerical methods:

- Flexibility for the choice of loss function;

- Larger solution space with flexible choice of deep neural networks;

d	σ	Method	Relative L^2 error ($\times 10^{-2}$)		
			u	∇u	$\text{diag}(\nabla^2 u)$
1	ReQU	DGM	34.9171	20.6788	34.3661
		MIM^1	0.5705	5.3709	0.5369
		MIM^2	1.2920	0.8129	1.9244
	ReCU	DGM	0.7603	0.4785	0.5977
		MIM^1	0.0991	0.7313	0.0128
		MIM^2	0.5035	0.5804	0.1229
2	ReQU	DGM	84.8708	85.8114	85.8954
		MIM^1	2.9393	1.9996	2.9443
		MIM^2	2.1820	2.5591	2.1383
	ReCU	DGM	2.5483	2.1856	2.4431
		MIM^1	1.5410	2.3865	1.5645
		MIM^2	5.5900	5.7440	5.8957
3	ReQU	DGM	168.1755	168.1697	169.3528
		MIM^1	4.0421	4.0987	3.8496
		MIM^2	7.7027	8.8787	9.1058
	ReCU	DGM	1.9132	1.4846	1.7970
		MIM^1	1.5410	2.3865	1.5645
		MIM^2	5.5900	5.7440	5.8957

Table 11: Relative L^2 errors for KdV equation defined in (14).

- Enforcement of exact boundary conditions;

- Better approximations of high-order derivations with almost the same cost.

Meanwhile, the deep mixed residual method also provides a better approximation for the PDE solution itself. These features make deep mixed residual method suitable for solving high-order PDEs in high dimensions.

Boundary condition is another issue which is important for solving PDEs by DNNs. Enforcement of exact boundary conditions not only makes the training process easier, but also improves the approximation accuracy; see [4, 8] for examples. The deep mixed residual method has the potential for imposing exact boundary conditions such as Neumann boundary condition, mixed boundary condition, and Robin boundary condition. All these conditions cannot be enforced exactly in deep Galerkin method. This shall be investigated in a subsequent work [29].

So far, in the deep mixed residual method, only experiences from classical numerical methods at the basic level are transferred into deep learning. We have seen its obvious advantages. To further improve the deep mixed residual method, we need to transfer our experiences from classical numerical analysis at a deeper level. For example, the choice of solution space relies heavily on the choice of residual in order to maximize the performance of least-squares finite element method [5]. Many other connections exist in discontinuous Galerkin method [10] and mixed finite element method [6]. For examples, since only first-order derivatives appear in the deep mixed residual method, ReLU works well for all time-independent equations we have tested but does not work well for KdV equation. Therefore, it deserves a theoretical understanding of the proposed method in the language of linear finite element method [20]. Another possible connection is to use the weak formulation of the mixed residual instead of least-squares loss, as done in deep learning by [38] and in discontinuous Galerkin method by [10]. Realizing these connections in the deep mixed residual method will allow for a systematic way to understand and improve deep learning for solving PDEs.

5. Acknowledgments

References

[1] Martino Bardi and Italo Capuzzo-Dolcetta, *Optimal control and viscosity solutions of Hamilton-Jacobi-Bellman equations*, Springer Science & Business Media, 2008.

[2] Christian Beck, Weinan E, and Arnulf Jentzen, *Machine learning approximation algorithms for high-dimensional fully nonlinear partial differential equations and second-order backward stochastic differential equations*, Journal of Nonlinear Science **29** (2019), no. 4, 1563–1619.

[3] Christian Beck, Lukas Gonon, and Arnulf Jentzen, *Overcoming the curse of dimensionality in the numerical approximation of high-dimensional semilinear elliptic partial differential equations*, arXiv preprint arXiv:2003.00596 (2020).

[4] Jens Berg and Kaj Nyström, *A unified deep artificial neural network approach to partial differential equations in complex geometries*, Neurocomputing **317** (2018), 28–41.

[5] Pavel Bochev and Max Gunzburger, *Least Squares Finite Element Methods*, Springer, Berlin, Heidelberg, 2015.

[6] Daniele Boffi, Franco Brezzi, and Michel Fortin, *Mixed Finite Element Methods and Applications*, Springer, Berlin, Heidelberg, 2013.

[7] J A González Cervera, *Solution of the black-scholes equation using artificial neural networks*, Journal of Physics: Conference Series **1221** (2019), 012044.

[8] Jingrun Chen, Rui Du, and Keke Wu, *A comprehensive study of boundary conditions when solving PDEs by DNNs*, arXiv preprint arXiv:2005.04554 (2020).

[9] Bernardo Cockburn, Bo Dong, and Johnny Guzman, *A hybridizable and superconvergent discontinuous galerkin method for biharmonic problems*, Journal of Scientific Computing **40** (2009), no. 1, 141–187.

[10] Bernardo Cockburn, George E. Karniadakis, and Chi-Wang Shu, *Discontinuous Galerkin Methods - Theory, Computation and Applications*, Springer-Verlag Berlin Heidelberg, 2000.

[11] Paul Adrien Maurice Dirac, *The principles of quantum mechanics*, no. 27, Oxford university press, 1981.

[12] Niccolo Discacciati, Jan S Hesthaven, and Deep Ray, *Controlling oscillations in high-order discontinuous galerkin schemes using artificial viscosity tuned by neural networks*, Journal of Computational Physics **409** (2020), 109304.

[13] Weinan E, Jiequn Han, and Arnulf Jentzen, *Deep learning-based numerical methods for high-dimensional parabolic partial differential equations and backward stochastic differential equations*, Communications in Mathematics and Statistics **5** (2017), no. 4, 349–380.

[14] Weinan E and Bing Yu, *The Deep Ritz Method: A Deep Learning-Based Numerical Algorithm for Solving Variational Problems*, Communications in Mathematics and Statistics **6** (2018), no. 1, 1–12.

[15] Howard Elman, David Silvester, and Andy Wathen, *Finite Elements and Fast Iterative Solvers: with Applications in Incompressible Fluid Dynamics*, Oxford University Press, 2014.

[16] Yuwei Fan, Lin Lin, Lexing Ying, and Leonardo Zepeda-Núñez, *A multiscale neural network based on hierarchical matrices*, Multiscale Modeling & Simulation **17** (2019), no. 4, 1189–1213.

[17] Carleo Giuseppe and Troyer Matthias, *Solving the quantum many-body problem with artificial neural networks*, Science **355** (2017), no. 6325, 602–606.

[18] Jiequn Han, Arnulf Jentzen, and Weinan E, *Solving high-dimensional partial differential equations using deep learning*, Proceedings of the National Academy of Sciences of the United States of America **115** (2018), no. 34, 8505–8510.

[19] Jiequn Han, Linfeng Zhang, and Weinan E, *Solving many-electron schrödinger equation using deep neural networks*, Journal of Computational Physics **399** (2019), 108929.

[20] Juncai He, Lin Li, Jinchao Xu, and Chunyue Zheng, *Relu deep neural networks and linear finite elements*, arXiv preprint arXiv:1807.03973 (2018).

[21] Kaiming He, Xiangyu Zhang, Shaoqing Ren, and Jian Sun, *Deep residual learning for image recognition*, CoRR **1512.03385** (2015).

[22] _____, *Deep residual learning for image recognition*, 2016 IEEE Conference on Computer Vision and Pattern Recognition (CVPR) **2** (2016), 770–778.

[23] C. John Hull, *Options, futures and other derivatives*, Upper Saddle River, NJ: Prentice Hall,, 2009.

[24] Martin Hutzenthaler, Arnulf Jentzen, Thomas Kruse, and Tuan Anh Nguyen, *A proof that rectified deep neural networks overcome the curse of dimensionality in the numerical approximation of semilinear heat equations*, arXiv preprint arXiv:1901.10854 (2019).

[25] Yuehaw Khoo, Jianfeng Lu, and Lexing Ying, *Solving for high-dimensional committor functions using artificial neural networks*, Research in the Mathematical Sciences **6** (2019), 1.

[26] Diederik P Kingma and Jimmy Ba, *Adam: A method for stochastic optimization*, arXiv preprint arXiv:1412.6980 (2014).

[27] Randall J. LeVeque, *Finite Difference Methods for Ordinary and Partial Differential Equations: Steady-State and Time-Dependent Problems*, Society for Industrial and Applied Mathematics, 2007.

[28] Ke Li, Kejun Tang, Tianfan Wu, and Qifeng Liao, *D3M: A Deep Domain Decomposition Method for Partial Differential Equations*, IEEE Access **8** (2019), 5283–5294.

[29] Liyao Lyu, Keke Wu, Rui Du, and Jingrun Chen, *Enforcing exact boundary and initial condtions in the deep mixed residual method*, in preparation (2020).

[30] Lin Mu, Junping Wang, and Xiu Ye, *A weak Galerkin finite element method with polynomial reduction*, Journal of Computational and Applied Mathematics **285** (2015), 45–58.

[31] Adam Paszke, Sam Gross, Soumith Chintala, Gregory Chanan, Edward Yang, Zachary DeVito, Zeming Lin, Alban Desmaison, Luca Antiga, and Adam Lerer, *Automatic differentiation in PyTorch*, Oct 2017, [Online; accessed 13. May 2020].

[32] Maziar Raissi, *Deep hidden physics models: deep learning of nonlinear partial differential equations*, Journal of Machine Learning Research **19** (2018), no. 1, 932–955.

[33] Maziar Raissi, Paris Perdikaris, and George Em Karniadakis, *Physics-informed neural networks: A deep learning framework for solving forward and inverse problems involving nonlinear partial differential equations*, Journal of Computational Physics **378** (2019), 686–707.

[34] Jie Shen, Tao Tang, and Li-Lian Wang, *Spectral methods: algorithms, analysis and applications*, vol. 41, Springer Science & Business Media, 2011.

[35] Justin A Sirignano and Konstantinos Spiliopoulos, *DGM: A deep learning algorithm for solving partial differential equations*, Journal of Computational Physics **375** (2018), 1339–1364.

[36] Yating Wang, Siu Wun Cheung, Eric T Chung, Yalchin Efendiev, and Min Wang, *Deep multiscale model learning*, Journal of Computational Physics **406** (2020), 109071–109071.

[37] Jue Yan and Chi-Wang Shu, *Local Discontinuous Galerkin Methods for Partial Differential Equations with Higher Order Derivatives*, Journal of Scientific Computing **17** (2002), no. 1, 27–47.

[38] Yaohua Zang, Gang Bao, Xiaojing Ye, and Haomin Zhou, *Weak adversarial networks for high-dimensional partial differential equations*, Journal of Computational Physics **411** (2020), 109409.

[39] Yinhao Zhu, Nicholas Zabaras, Phaedon-Stelios Koutsourelakis, and Paris Perdikaris, *Physics-constrained deep learning for high-dimensional surrogate modeling and uncertainty quantification without labeled data*, Journal of Computational Physics **394** (2019), 56–81.